Int J Adv Manuf Technol (2012) 58:949–967
DOI 10.1007/s00170-011-3438-8

ORIGINAL ARTICLE

Surface finish prediction models for precision grinding of silicon

Abdur-Rasheed Alao · Mohamed Konneh

Received: 12 April 2011 / Accepted: 6 June 2011 / Published online: 23 June 2011

Abstract Conventional grinding of silicon substrates results in poor surface quality unless they are machined in ductile mode on expensive ultra-precision machine tools. However, precision grinding can be used to generate massive ductile surfaces on silicon so that the polishing time can be reduced immensely and surface quality improved. However, precision grinding has to be planned with reliability in advance and the process has to be performed with high rates of reproducibility. Therefore, this work reports the empirical models developed for surface parameters R_a, R_{max}, and R_t with precision grinding parameters, depths of cut, feed rates, and spindle speeds using conventional numerical control machine tools with Box–Behnken design. Second-order models are developed for the surface parameters in relation to the grinding parameters. Analysis of variance is used to show the parameters as well as their interactions that influence the roughness models. The models are capable of navigating the design space. Also, the results show large amounts of ductile streaks at depth of cut of 20 μm, feed rate of 6.25 mm/min, and spindle speed of 70,000 rpm with a 43-nm R_a. Optimization experiments by desirability function generate 37-nm R_a, 400-nm R_{max}, and 880-nm R_t with massive ductile surfaces.

Keywords Precision grinding · Box–Behnken design · Silicon · Surface roughness parameters · Empirical models · Analysis of variance

1 Introduction

Silicon substrates are hard–brittle materials and are difficult to machine to good surface finishes. However, they find important applications in electronics, semi-conductor, and optical industries. Fang and Venkatesh [1] have reported that silicon, which constitutes 90% of all semiconductors, is used to make important devices in micro-electro mechanical systems, integrated circuits (IC) chips, and optical components in high-resolution thermal imaging systems. Because of the exacting requirements on the finishing technique for these applications, close tolerance and good surface finishes are critical. To meet the surface quality requirements in these industries, the machined surfaces must be crack-free requiring ductile mode machining. Ductile mode machining is a phenomenon whereby silicon and other brittle materials are machined in a ductile manner rather than brittle manner such that extensive micro-cracks can be minimized.

Ductile machining can be realized using two phenomena. These are single-point diamond turning (SPDT) and ultra-precision grinding (UPG) both of which are performed on ultra-precision machine tools. Fang and Venkatesh [1] have applied SPDT to cut silicon and optical glass in ductile modes after analyzing the cutting mechanism. They reported that for turned silicon surfaces with 23.8-nm R_a and 140-nm R_{max}, mirror surfaces of 1-nm R_a were

A.-R. Alao (✉)
Advanced Manufacturing and Materials Processing Technology (AMMPT) Laboratory, Department of Engineering Design & Manufacture, Faculty of Engineering Building,
University of Malaya,
50603 Kuala Lumpur, Malaysia
e-mail: alaoar@siswa.um.edu.my

M. Konneh
Department of Manufacturing and Materials Engineering,
International Islamic University Malaysia (IIUM),
P.O. Box 10, 50728 Kuala Lumpur, Malaysia
e-mail: mkonneh@iium.edu.my

achieved repeatedly. Shibata et al. [2] have used SPDT to obtain a mirror finished surface of 20-nm R_{max} at 100-nm cut depth on silicon. Venkatesh et al. [3] have investigated machining of single-crystal silicon using a single-crystal diamond tool of zero rake and 0.75 μm nose radius. They reported a surface roughness of 1-nm R_a at a depth of cut of 1 μm, feed of 0.4 mm/min, and a cutting speed of 400 m/min.

Some researchers have also used UPG to machine brittle materials. Komanduri et al. [4] have written extensively on the advancement in the technologies of grinding brittle materials and ultra-precision machining of both ductile and brittle materials over a period of past two decades. They state that all aspects of grinding systems have advanced including new abrasives, new bonding methods, new controls, new machine tools, new processes, and their supply to the grinding zone. Extremely rigid, high-power, high-speed, and high-performance machine tools have been built to handle machining of brittle materials. Various grinding wheels have been developed including metal-bonded grinding wheels, resin-bonded grinding wheels, etc., and new processes of dressing them have evolved. One of such grinding techniques, called electrolytic in-process dressing (ELID), is the new way for mirror finishing of silicon wafers. The importance of using ELID dressing process to give a high surface quality has been discussed by Rahman et al. [5]. They have reported that grinding with super abrasive wheels is an excellent way to produce ultra-precision surface finish on brittle materials. However, super abrasive diamond grits require high wheel grade (i.e., higher bonding strength) while grinding, which metal-bonded grinding wheels could offer. Truing and dressing of the wheels are the major problems, and they tend to glaze because of wheel loading. When grinding with super abrasive wheels, wheel loading could be avoided by dressing periodically to obtain continuous grinding. ELID is the most suitable process for dressing metal-bonded grinding wheels during the grinding process. Zhang et al. [6] have therefore shown the application of ELID on grinding structural ceramics with cast iron-bonded diamond grinding wheels to produce high material removal rates (MRR) since the grain protrusion from the wheel size is maintained constantly. The results show the reduction in normal grinding force and the increase in MRR using ELID grinding.

Analytical model explaining ductile mode machining of brittle material with SPDT has been carried out by Blackley and Scattergood [7]. This model provides critical depth of cut that must not be exceeded to obtain mirror surfaces on brittle materials. They also provide the maximum feed rate that can be used to achieve fully ductile surfaces. König and Sinhoff [8] have provided theoretical requirements for the realization of ductile mode grinding of optical glasses. The criteria for realizing ductile regime grinding, according to them, are that the depth of cut must not exceed certain critical depth of cut and the protruding grains in the grinding wheels must be flattened. The range of the critical depth of cut for the realization of fully ductile mode machining on various hard and brittle materials has been found to be between 50 nm to 1 μm, depending on the machining directions and coolants used [9]. However, this range can only be set on the expensive ultra-precision machine tools. When ductile mode machining of brittle materials is achieved, nanometer order surface roughness is obtained and subsurface damage is minimized.

However, because of the prohibitive cost of ultra-precision machine tools coupled with the requirement for the skilled manpower for the operation of these machine tools, the use of ductile mode machining concept has been limited to the production of optical lenses in the optical industry, although its application has been known by industries. Therefore, because of these reasons, research trends have shifted to the use of conventional machine tools to machine brittle materials like silicon using a machining phenomenon termed partial ductile mode machining. Partial ductile mode machining is a precision machining technique where 100% ductile mode machining is not achievable. Partial ductile mode machining focuses on grinding conditions that generate massive ductile surfaces followed by a polishing process. It is expected that the polishing time can be reduced greatly and the surface quality improved on ground surfaces with massive ductile-streaked surfaces. Therefore, partial ductile mode machining appears to be more attractive alternative to the optical and semi-conductor industries because the grinding wheels and the machines are reasonably priced.

Several authors have reportedly generated some partial ductile surfaces on different brittle materials. To mention but a few, Ong and Venkatesh [10] have reported generating qualitatively 85% ductile surfaces on ground Pyrex glass samples with a fine-grit resin-bonded diamond cup wheels on a conventional surface grinder. The surface roughness values have been established in the range of 53–82 nm. Zhong [9] has obtained ductile or partial ductile surfaces of brittle materials with computerized numerical control (CNC) machine tools. The conclusions from his works show that massive ductile streaks could be generated by proper selection of cutting conditions. Venkatesh et al. [11] have investigated the amounts of ductile streaks produced during diamond grinding of silicon and glass. Considerable amounts of ductile streaks on silicon, germanium, and glass have been reportedly obtained. They have concluded that by correct selection of the grinding conditions, larger amounts of ductile streaks could be achieved. Venkatesh and Izman [12] have converted CNC machine into a high-speed machine by attaching its spindle with an ultra-precision high-speed jig grinder to machine IC chips with resin-bonded diamond wheels (grinding pins). Diamond

pins have also been used by Izman and Venkatesh [13] to produce flat surfaces on glass surfaces by vertical surface grinding with the use of an NSK Planet 1500 attached to the spindle of a CNC machine. Furthermore, spherical chips have been reportedly generated for glass by Venkatesh et al. [14] at 5 μm under wet conditions in surface grinding with diamond pins. The central hole ultrasonically drilled on the diamond pin has enabled the formation of the spherical chips. Also, Liu et al. [15] have reported that resin-bonded grinding wheels outperform metal- or vitrified-bonded wheels in terms of reduction in both the surface roughness and subsurface damage during grinding of ceramics.

In all the works reviewed above, many efforts have been expended on the grinding conditions that could generate large amounts of ductile streaks using resin-bonded diamond mounted wheels with traditional method of experimentation to obtain partial ductile surfaces, while little attention has been paid to the optimization of the precision grinding process. Therefore, in order to have good surface quality on ground silicon surfaces, it becomes necessary to employ optimization techniques to find optimal grinding conditions and develop workable models between the roughness and the grinding parameters in order to plan the process in advance with high rates of reproducibility. Response surface methodology (RSM) can conveniently be used for this purpose.

Surface roughness is a widely used index of a product's surface quality and, in most cases, a technical requirement for mechanical products. The final surface roughness of a precision ground surface is a combination of both the natural and ideal surface roughness. The ideal roughness is more reliably predicted from empirical equations. Among the surface roughness parameters, the average surface roughness (R_a) is the most commonly used. Since surfaces generated by machining are usually characterized by the amplitude parameters, spacing parameters, and hybrid parameters, consideration of only one roughness parameter like R_a is not sufficient to solely describe the surface quality [16]. Hence, surface parameters R_a, R_{max}, and R_t have been selected for this study. This paper therefore reports prediction models developed for roughness parameters R_a, R_{max}, and R_t in terms of depths of cut, feed rates, and spindle speeds based on Box–Behnken design. Furthermore, the roughness parameters are optimized to provide the optimum precision grinding conditions necessary to generate massive ductile surface on precision ground silicon.

2 Mechanism of material removal in precision grinding of silicon

Silicon is a hard material because it features low density and low mobility of dislocations. It is also a brittle material because its fracture toughness is greater than its yield strength so fracture occurs before it starts to undergo plasticity. According to Inasaki [17], silicon features low ductility and fracture toughness at room temperature and standard pressure so that fracture occurs once the atomic forces are exceeded. Because of the low fracture toughness, conventional grinding of silicon results into brittle fracture (the fracture toughness of silicon is low, so the yield strength is lower). This then requires postmachining operations like polishing in order to obtain the desired surface finish. Polishing is a time consuming operation, and therefore, the polishing time must be reduced. However, silicon can be made to undergo plastic deformation only under high hydrostatic pressure at room temperature since it has been reported that the mode of deformation (elastic or plastic) of any materials depends on the state of stress. From the works of Bridgman [18], it has been proven that in order for brittle materials to deform plastically, a considerable hydrostatic stress and/or temperature are required. When plastic deformation takes place in silicon, the covalent diamond structure of silicon (α-silicon) can be transformed into a metallic body-centered tetragonal structure (β-tin structure) [19]. To realize plastic deformation of silicon in a machining operation, nonconventional machining technique must be employed. Precision grinding is a nonconventional machining method which is capable of enabling the tendency to deform silicon in ductile mode by generating large amounts of ductile streaks to aid a reduction in polishing time and an improvement on surface quality. Precision grinding is a finishing process to produce components with high surface quality and accuracy. The accuracy required is at the submicron or nanometric levels.

Figure 1 shows how a material can be removed in brittle materials like silicon in a precision grinding process. It is shown on this figure that the precision grinding operation is being accomplished through negative rake angle. Fang and Zhang [20] explained that while cutting brittle materials at 0° or negative rake angle, the cutting action is actually

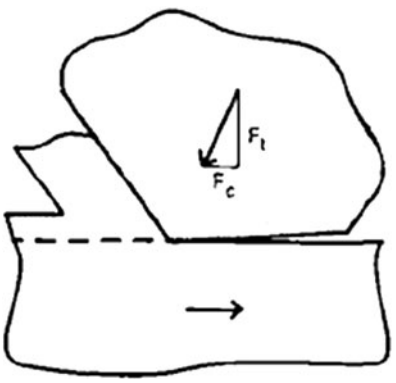

Fig. 1 Material removal process at the tool–workpiece interaction in precision grinding of silicon

being carried out in large negative effective angle. It is this effective angle that permits the generation of the necessary hydrostatic pressure to enable plastic deformation of brittle materials. When precision grinding (micro-grinding) occurs, the thrust force may be larger than the cutting force as shown in Fig. 1. The chips formed as a result of precision grinding operation may be continuous indicating ductile material removal process [21]. However, discontinuous chips have also been reported as indicative of ductile material removal process of brittle materials. Liu et al. [22] observed shorter chips on soda-lime glass with very smooth surfaces in ductile mode. Also, Liu et al. [23] in their investigation on ductile mode cutting of soda-lime glass reported that discontinuous chips were produced even though the cutting was in ductile mode with 20.3-nm R_a. Consequently, the formation of continuous chips in a ductile cutting operation is not a sole criterion to determine the existence of ductile or brittle modes in a precision grinding process. Therefore, surface observations augmented with surface roughness parameters measurements continue to be the preferred approach to determine ductile and brittle material removal in precision grinding of silicon.

Miyashita [24] classified precision grinding (micro-grinding) operation as a gap between polishing and conventional grinding in terms of specific material removal rate and the grain size requirements (Fig. 2). It can be seen on this figure that precision grinding requires less polishing action than conventional grinding. Practical realization of precision grinding process of brittle materials like silicon requires very small grain size and very small indentations [25]. However, to realize a small indentation in reality, it requires high wheel rotation and/or slow feed rate. In such a condition, it is known that the mode of grinding is often ductile for most materials. This shows that in precision grinding, depths of cut, feed rates, and wheel spindle speeds can have an important influence on the material removal process. Furthermore, Zhong [9] stated that ductile and brittle modes of deformation can occur in the same brittle material and the transition between them can be controlled by changing the machining conditions. It is therefore important to determine precision grinding conditions

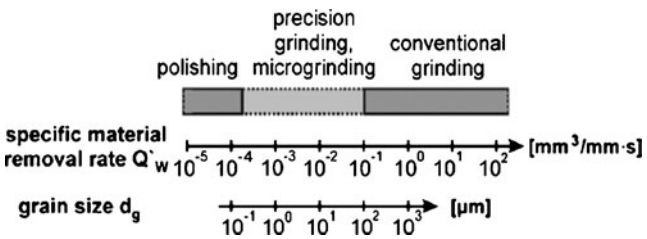

Fig. 2 Classification of precision and micro-grinding with respect to polishing and conventional grinding based on specific material removal rate and grain size

necessary to generate massive ductile surfaces on silicon so that the polishing time can be reduced and the surface quality improved. Generating massive ductile surfaces on precision ground surfaces can be realized by proper selection of grinding conditions. It is highly desirable to also optimize these conditions through the use of Box–Behnken method.

3 Box–Behnken method

IC chip manufacturers often go for precision grinding of silicon die and then carry out ductile mode polishing for failure diagnosing analysis of the chips [12]. In order to evaluate the efficiency of the precision grinding operation, there is a need to relate depths of cut, feed rates, and spindle speeds to the surface roughness parameters. Process modeling is the scientific basis for this. Surface quality is one of the measures of process efficiency. To achieve the modeling of precision grinding process, response surface methodology (RSM) is always utilized. Montgomery et al. [26] define RSM as a collection of mathematical and statistical techniques that are useful for modeling and analysis in applications where a response of interest is influenced by several factors and the objective is to optimize this response. Among RSM classes, Box–Behnken design has found broad application because of its simplicity. Box–Behnken design requires only three levels, and it is based on the combination of the factorial with incomplete block designs for each independent parameter. This procedure creates designs with desirable statistical properties but most importantly with only a fraction of the experiments required for three-level factorials.

Just as in the case of precision grinding operation, in other manufacturing processes, there is a relationship between a response y and a set of controllable factors $\{x_1, x_2, \ldots, x_n\}$. In some systems, the functional relationship

Table 1 Physical and mechanical properties of silicon [4]

Lattice structure	Diamond cubic
Bond type	Covalent
Lattice constant (Å)	5.4307
Density (g/cm^3)	2.328
Melting point (°C)	1410
Young modulus (N/mm^2)	188,400
Poisson's ratio (v)	0.28
Vicker's hardness, H_v (kg/mm^2)	950
Mohs hardness	6.5
Fracture toughness (MPa mm$^{1/2}$)	15
Resistivity at 300 K	2.3×10^5
Energy gap (eV)	1.1

between y and x values might be known. Then, a model can be written in the form of:

$$y = f(x_1, x_2, ..., x_n) + \varepsilon \quad (1)$$

where ε represents error observed in the response y. Denoting the expected surface by $E(y) = f(x_1, x_2, ..., x_n) = \widehat{y}$ in Eq. 1, then the surface represented by

$$\widehat{y} = f(x_1, x_2, \ldots, x_n) \quad (2)$$

is called the response surface. In most RSM problems, the form of the relationship between the output and the independent factors is unknown. So, the first step is to find an appropriate approximation for the true functional relationship between y and the independent factors. Usually, a second-order model is used in RSM [26].

$$\widehat{y} = \beta_0 + \sum_{i=1}^{k} \beta_i x_i + \sum_{i=1}^{k} \beta_{ii} x_i^2 + \sum_i \sum_j \beta_{ij} x_i x_j + \varepsilon \quad (3)$$

where βs and ε are the coefficients and error to be determined from the least square method, respectively. The second-order model is normally used where the response function is unknown, nonlinear or three levels are selected for independent factors.

Empirical modeling and optimization of the plunge centerless grinding process have been performed by Krajnik et al. [27] using RSM as a tool that integrates design of experiments, regression modeling, and basic optimization. The single-objective optimization is solved by nonlinear programming and genetic algorithm. The ground surface roughness is most significantly affected by the wheel dressing condition and the geometrical grinding gap setup factor and the wheel speed. Alao and Konneh [28] have developed the procedural frameworks for the development, validation, and acceptability of empirical models using RSM. They have therefore applied the steps to developing an R_t model for precision grinding of silicon. It is shown that the procedural modeling frameworks have worked well for the R_t model developed.

3.1 Multiple-objective optimizations

In this study, the influences of depths of cut, feed rates, and spindle speeds are investigated on the surface finish parameters R_a, R_{max}, and R_t (multiple responses) and the optimum precision grinding conditions are determined simultaneously by minimizing all the roughness parameters. By doing so, it is envisaged that low surface roughness correlate well with massive ductile streaks. A desirability function based on simultaneous optimization method, popularized by Derringer and Suich [29], is used in this study. The approach first converts individual response Y_i (R_a, R_{max}, and R_t) into an individual desirability function that varies from 0 and 1 ($0 \le d_i \le 1$). Here $d(Y_i)=0$ and $d(Y_i)=1$ represent respectively a completely undesirable and an ideal response value. The individual desirabilities are then coupled together using the geometric mean that gives the overall desirability D as in Eq. 4 below,

$$\begin{aligned} D &= \sqrt[n]{d_1 \times d_2 \times \ldots \times d_n} \\ &= (d_1 \times d_2 \times \ldots \times d_n)^{\frac{1}{n}} \end{aligned} \quad (4)$$

where n is the number of responses. The geometric mean of overall desirability for this study is as given in Eq. 5,

$$D = (d_{R_a} \times d_{R_{max}} \times d_{R_t})^{\frac{1}{3}} \quad (5)$$

Depending on the optimization objectives like minimization, maximization, and assignment of a target value, different desirability functions $d(Y_i)$ can be applied. In our work, the objective was to minimize R_a, R_{max}, and R_t, and the desirability function used is given below,

$$d(Y_i) = \begin{cases} 1 & \text{if } Y_i < T \\ \left(\frac{U - Y_i}{U - T}\right)^r & \text{if } T \le Y_i \le U \\ 0 & \text{if } Y_i > T \end{cases} \quad (6)$$

where U is the upper limit, T is the target value, and r is the weight. Assigning 1 to r makes the desirability function to be linear. If r is assigned a value greater 1, the desirability function tends to be near the target value, but if r is between 0 and 1, it makes the target value less important. In this work, r is taken as 1 to make the desirability function linear.

4 Experimental details

4.1 Work and tools materials

The workpiece materials that have been precision ground are mono-crystalline silicon samples. Table 1 shows the physical and mechanical properties of monocrystalline silicon. The samples were cut precisely into dimensions 15×15×6 mm. Tool materials are 5–6-mm-diameter Winter-made resin-bonded diamond grinding wheels (Fig. 3). The shape, grit size, concentration, diameter, height, and diamond thickness of the grinding wheel are 1A1W, 64 μm, C100, 5 mm and 1.5 mm respectively.

4.2 Experimental equipment and instruments

The equipment and instruments that have been used in the experimental trials include a five-axis DMU 35M DECKEL MAHO numerical control (NC) milling and an ultra-precision high-speed jig grinder (NSK PLANET 850). The details of the machine tool, grinding wheels, grinding conditions, dresser, and dressing condition are shown in

Fig. 3 A 5-mm-diameter resin-bonded grinding wheel used during experimentation with specification 1A1 W-5-6 D64 K-888 RY C100

Table 2. Figure 4 shows the experimental setup for this study. Mitutoyo Surftest (SV-514) was used for surface roughness measurements, while optical microscope and JSM-5600 scanning electron microscope (SEM) were used to observe the ground surfaces.

4.3 Experimental setup and procedure

Precision grinding experiments have been carried out on the vertical five-axis NC milling whose spindle has been upgraded by attaching the Planet 850 to enhance the spindle speed. Pre-grinding operations have been carried out on each silicon sample to ensure flatness of the workpiece before carrying out any precision grinding trials. Holes have been drilled at the centers of the grinding pins by ultrasonic technique to prevent zero velocity. Coolant flow rate has been maintained at 7 L/min to minimize the effects of stalling and dragging marks [13]. Before trying out a new grinding condition, a grinding pin was dressed on an alumina dressing stick shown in Fig. 4.

4.4 Roughness measurement procedures

Average roughness (R_a), maximum peak-to-valley height within a sampling length (R_{max}), and maximum peak-to-valley height within an evaluation length (R_t) have been measured in this study using Mitutoyo Surftest (SV-514) in transverse direction and perpendicular to the machined surface on silicon ground samples, at 0.25-mm cutoff length (sampling length) and 1.25-mm evaluation length. On each pass on the silicon sample, three readings for R_a, R_{max}, and R_t were recorded and the average readings computed. Figure 5 shows the surface roughness measurement being carried out.

Mathematically denoted by Eq. 7, R_a is one of the statistical parameters for inspection and tolerancing of machined surface. These statistics are defined in Fig. 6, where R_a is the arithmetic mean deviation, L is the sampling length, and y is the ordinate of the of profile curve which is

Table 2 Machine tool, grinding wheels, precision grinding, and dressing conditions

Machine tool	A 5-axis DMU 35M DECKEL MAHO numerical control (NC)
	X,*Y*,*Z* resolution, 0.001 mm
	Motor power, 45 kW
	Maximum speed, 6,500 rpm
	Maximum coolant flow rate, 7 L/min
Ultra-precision high-speed jig grinder	Planet 850 jig grinder
	Maximum spindle speed, 100,000 rpm
	Motor power, 1.47 kW
Grinding wheel (grinding pin)	Resin-bonded diamond grinding wheel diameter, 5 mm
	Shape, 1A1W
	Concentration, 100% concentration of diamond grains
	Average grain size, 64 μm
Grinding coolant	Castrol Miracol 80 diluted in water with a ratio 1:50
Precision grinding conditions	
Depth of cut (a)	5, 12.5, and 20 μm
Feed rate (f)	2.5, 6.25, and 10 mm/min
Spindle speed (n)	70,000, 80,000, and 90,000 rpm
Dresser and dressing conditions	
Dresser	Al_2O_3 bar (grade number 2)
Dressing conditions	a=10 μm, f=25 mm/min, n=50,000 rpm
	Number of passes=10

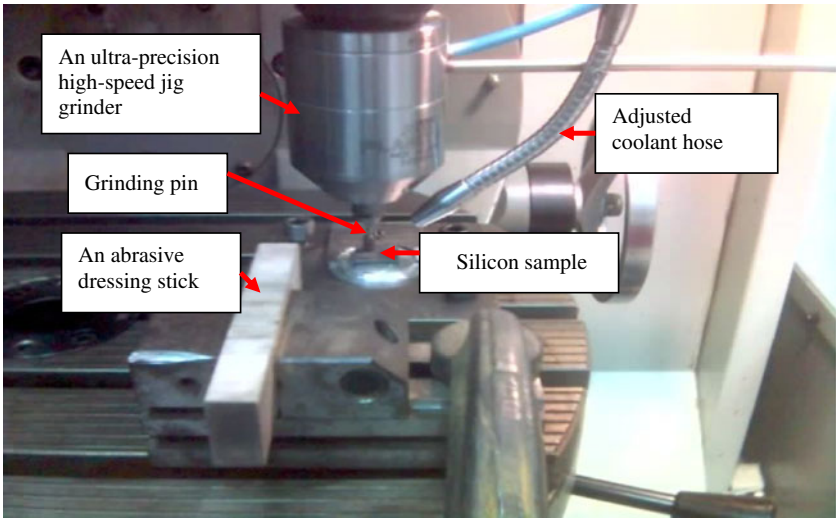

Fig. 4 Experimental setup showing a high-speed jig grinder unit attached on NC vertical milling spindle and the Al_2O_3 abrasive stick (grade Nr.2)

a function of x [30].

$$R_a = \frac{1}{L}\int_0^L |y(x)|dx \tag{7}$$

Figure 7 shows the statistics used to compute the maximum-to-peak height R_{max}. It can be computed using Eq. 8 below. In Eq. 8, Y_{max} and Y_{min} are the respective maximum profile peak and valley depth within the sampling length.

$$R_{max} = Y_{max} + Y_{min} \tag{8}$$

In a similar fashion, R_t (i.e., maximum-to-peak height from the entire evaluation length) can be computed using Eq. 9 below.

$$R_t = R_{p\ max} + R_{v\ max} \tag{9}$$

where $R_{p\ max}$ *and* $R_{v\ max}$ are the respective maximum profile peak and valley depth from the entire evaluation length.

4.5 Surface characterization

After performing precision grinding experiments, the ground surfaces were cleaned using ultrasonic technique and dried before being observed under optical microscope for surface topography. The surface resulting from the optimization experiments was coated in argon gas to make it conductive and then observed in scanning electron microscope to reveal its topography.

4.6 Experimental design

Box–Behnken design of experiment has been used in this research. Surface roughness in precision grinding has been found to be affected by machining variables, depths of cut, feed rates, and spindle speeds [31]. Matsuo et al. [32] have investigated the influence of depths of cut, feed rates, and wheel speeds on R_a and R_{max} in high-precision surface grinding of ceramics with super fine diamond cup

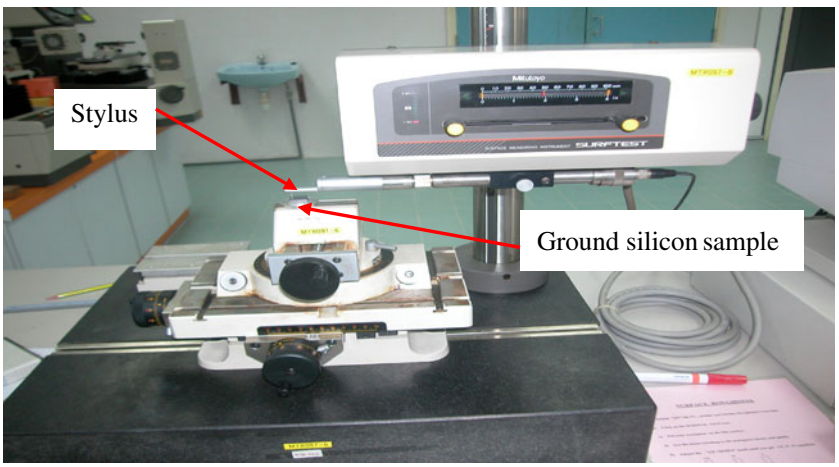

Fig. 5 Mitutoyo Surftest being used to measure surface roughness R_a, R_{max}, and R_t

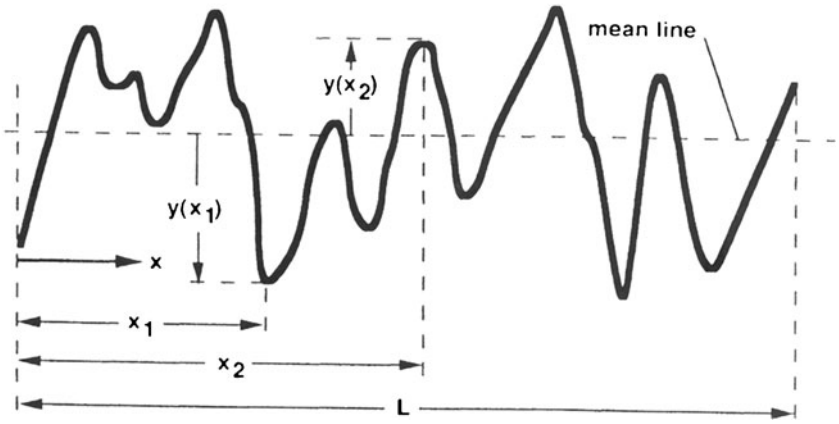

Fig. 6 Definition of parameters used to compute R_a [30]

wheels and reported some improvements on roughness parameters on ground ceramics when depth of cut and feed rate were reduced and wheel speed was increased. Routara et al. [33] have studied the main as well as the interactive effects of depths of cut, feed rates, and spindle speeds on five roughness parameters namely center line average roughness (R_a), root mean square roughness (R_q), skewness (R_{sk}), kurtosis (R_{ku}), and mean line peak spacing (R_{sm}) in CNC end milling of brass, aluminum, and mild steel. Furthermore, Masuzawa and Tönshoff [25] suggested that the conditions to realize precision grinding of brittle materials are low depth of cut, slow feed rate and high wheel rotation, and small grain size. Therefore, this study considered depths of cut, feed rates, and spindle speeds as the controllable factors. Furthermore, these parameters were set at three levels as shown in Table 2. The levels for the spindle speed were based on the workable range 70,000–90,000 rpm as specified by the manufacturer of the NSK Planet 850. The levels of feed rate and depth of cut were set based on the criteria suggested by Masuzawa and Tönshoff [25] in that low depth of cut and slow feed rate were the necessary conditions to establish precision grinding in brittle materials. So depth of cut and feed rate were set, respectively, within 5–20 μm and 2.5–10 mm/min (Table 2). The average grain size of the diamond grinding pins used in the investigation was 64 μm. This grit size corresponds to the range of wheel grit sizes in precision grinding process of brittle materials as classified by Miyashita [24] in his chat illustrated in Fig. 2. The grit size of this value lies within the region of precision grinding (10^0–10^2 μm) in Fig. 2.

Since a three-level factor requires all possible pairs of 2^2 designs, three factors at three levels would require a total possible pairs of $3(2^2)$ plus three replicates at the center making a total of 15 experimental trials. Equation 10 shows the linear codes −1, 0, 1 for the respective levels of the grinding parameters:

$$a = \frac{a_x - a_0}{a_1 - a_0} \tag{10}$$

$$f = \frac{f_x - f_0}{f_1 - f_0}$$

$$n = \frac{n_x - n_0}{n_1 - n_0}$$

where a, f, and n represent the coded levels of the grinding parameters and a_x, f_x, and n_x the actual values determined from the equation. The Box–Behnken experimental design and results obtained from the experiments are shown in Table 3.

5 Results and discussion

5.1 Ductile and fracture images of ground silicon surfaces

Table 3 shows the Box–Behnken design experiments and the results for this study. Each roughness response has been

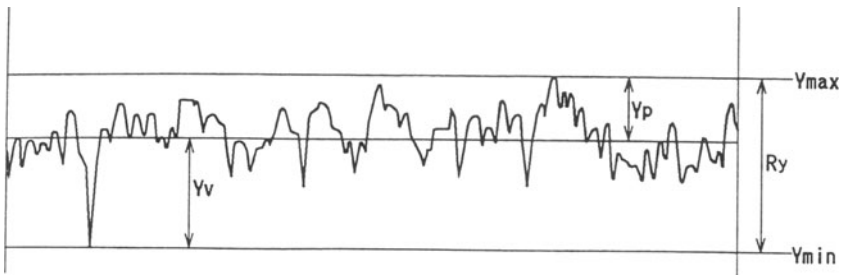

Fig. 7 Parameters used in computing R_{max} and R_t

Table 3 Box–Behnken experimental design

Experimental trial	Grinding parameter			Surface roughness parameter		
	a (μm)	f (mm/min)	n (rpm)	R_a (μm)	R_{max} (μm)	R_t (μm)
1	12.5	2.50	70,000	0.047	0.423	0.883
2	20.0	6.25	70,000	0.043	0.460	0.987
3	5.0	2.50	80,000	0.093	0.830	1.893
4	5.0	6.25	70,000	0.057	0.493	1.063
5	20.0	6.25	90,000	0.070	0.657	1.447
6	12.5	6.25	80,000	0.107	0.840	1.777
7	12.5	10.00	70,000	0.060	0.547	1.047
8	12.5	2.50	90,000	0.057	0.520	1.130
9	12.5	6.25	80,000	0.110	0.827	1.765
10	20.0	2.50	80,000	0.100	0.935	2.185
11	12.5	10.00	90,000	0.080	0.667	1.287
12	5.0	10.00	80,000	0.150	1.358	2.790
13	12.5	6.25	80,000	0.104	0.853	1.830
14	5.0	6.25	90,000	0.087	0.707	1.340
15	20.0	10.00	80,000	0.105	0.950	1.778

measured three times, and the average value is reported in Table 3. Two kinds of surfaces are generated in this research: partial ductile and fully fractured surfaces. As can be seen in this table, the lowest roughness (43-nm R_a, 460-nm R_{max}, and 987-nm R_t) is observed, giving massive ductile streaks in this study with grinding condition depth of cut of 20 μm, feed rate of 6.25 mm/min, and spindle speed of 70,000 rpm. Fully fractured mode is also noticed in this study having the highest roughness (150-nm R_a) with the condition depth of cut of 5 μm, feed rate of 10 mm/min, and spindle speed of 80,000 rpm. Figure 8 shows the two images from the optical microscope. The discrepancy in the surfaces generated and the difference in the roughness values can be attributed to the different grinding conditions, the conicity, and the small undeformed chip thickness at lower depth of cut of the grinding pin. When feed rate changes from 6.25 to 10 mm/min and spindle speed is increased from 70,000 to 80,000 rpm, friction between the grinding pin and the silicon sample is developed. This tends to lead to mechanical deformation of the silicon because the grinding pin is very slim as suggested by Masuzawa and Tönshoff [26]. The frictional effect generated as a consequence of increased feed rate and spindle speed does not lead to thermal damage of the workpiece materials in the grinding zone and consequently does not influence the material removal process because Inasaki [17] has reported that the thermal conductivity of silicon is 84 W/mK. Its thermal conductivity is higher than that of steel. The relatively high thermal conductivity of silicon coupled with low coefficient of friction and high thermal conductivity of diamond and the use of coolant enable cooler grinding without thermal damage of the workpiece materials. So, the poor surface finish observed is due to

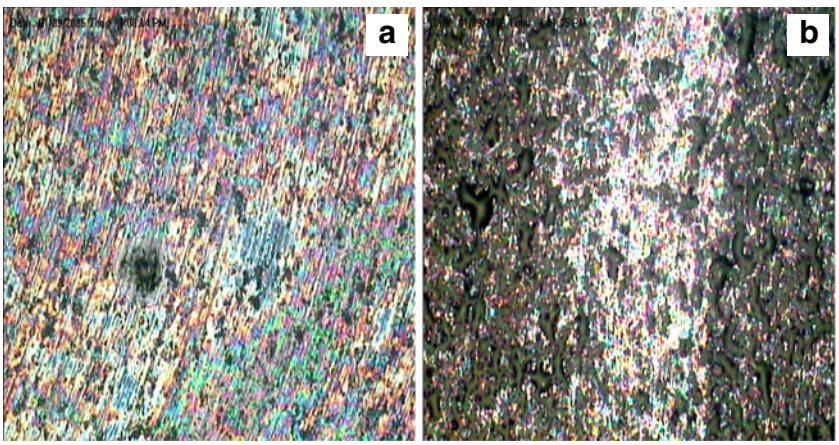

Fig. 8 Images of silicon ground surfaces: **a** large amount of ductile streaks with 43-nm R_a, 460-nm R_{max}, and 987 nm R_t and grinding conditions depth of cut of 20 μm, feed rate of 6.25 mm/min, and spindle speed of 70,000 rpm; **b** fully fractured surfaces of 150-nm R_a, 1.358-nm R_{max}, and 2.790-nm R_t with the condition depth of cut of 5 μm, feed rate of 10 mm/min, and spindle speed of 80,000 rpm

the increase in feed rate and spindle speed which in turn lead to mechanical strain of the silicon.

In addition to the point made above, other reason why more massive ductile streaks are formed on ground silicon at 20 μm than at 5 μm may be due to the conicity of the grinding pin. Traditionally, grinding pins are used for internal grinding and the slight conicity in them is to provide the grinding relief. When the grinding pins are adapted to surface grinding, the conical shape becomes more pronounced. Since it has been established by Venkatesh et al. [11] that the conical track of the grinding pin produces more ductile streaks than the central track when it is adapted to surface grinding, it is reasonable to assume that more conical configuration will touch the silicon surface at 20 μm than at 5 μm (see Fig. 9). It therefore becomes imperative that more ductile streaks are expected at 20 μm than at 5 μm while setting other parameters constant. Fang [34] noted that when cutting is done at small undeformed chip thickness (smaller undeformed chip thickness is obtained at 5 μm than at 20 μm), the cutting operation is being performed within the domain of large negative tool rake angles. Plowing can be formed on the machined process resulting in a poor surface finish. The ground silicon surfaces of other conditions in Table 2 fall within these two extreme surfaces.

5.2 Development of surface finish models

The procedures for developing the surface finish models in this study have been well detailed by Alao [35]. According to Alao and Konneh [28], the development of RS models include formulating problems, checking the response data for any transformation need, fitting of the input and output variables to know whether the relationship between them is linear, linear and two-factor interaction (2FI), second-order or higher-order function and investigating the p values. The p value of an observed value t_{observed} of some random variable T used as a test statistic is the probability that, given that the null hypothesis is true, T will assume a value as or more unfavorable to the null hypothesis as the observed value t_{observed} in the analysis of variance (ANOVA). So the p value represents the significance of a result, the smaller the p value in accordance with the set confidence interval, the more significant the result. Assessments of the quality of models include checking the lack of fit to make sure that it is not significant indicating that the data fit well in the models and evaluation of the coefficients of determination (R^2 and adjusted R^2). R^2 is a measure of the amount of reduction in variability of a response by using regression variables. However, Montgomery et al. [26] explain that R^2 is not a good statistic since its value can be artificially inflated by adding insignificant model terms. Adjusted R^2 $\left(R^2_{\text{adj}}\right)$ is a better statistical measure of the amount of observed variability in the response since its value will only increase if the additional terms are statistically significant. For models to be adequate and accurate, it is suggested that R^2_{adj} should be greater or equal to 70%.

Also, errors that arise during experimentation should be investigated by means of verifying their compliance with normal distribution criterion; they should also be verified to determine their compliance to having a constant variance; they should also be checked to know if they have a mean of zero; and, finally, experimental errors should be checked to know whether they are independent of one another. All these are determined via residual plots.

Based on the experimental results in Table 3 and the above modeling procedures, second-order equations have been found to be most suitable relating the roughness parameters and the precision grinding parameters depths of cut, feed rates, and spindle speeds using Design Expert. Equations 11–13 are the developed surface finish models. The significance of the model factors has been carried out by the analysis of variance (ANOVA). As can be seen in Eq. 11, R_a model does not require any response transformation, whereas in Eqs. 12 and 13, inverse square root

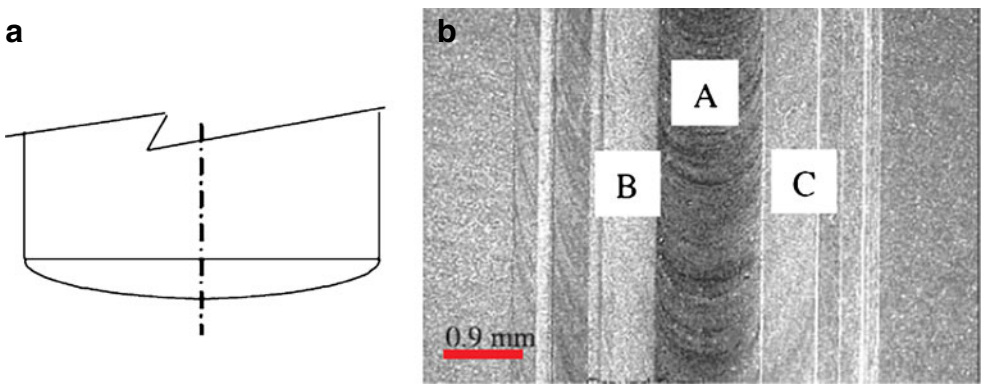

Fig. 9 **a** Exaggerated conicity of grinding wheel. **b** The resulting grinding track [11]

power transformation has been applied to the R_{max} and R_t models.

$$R_a = -3.04215 + 0.00173889a + 9.04444 \times 10^{-3}f + 7.66589 \times 10^{-5}n - 4.62222 \times 10^{-4}af - 4.72321 \times 10^{-10}n^2 \quad (11)$$

$$\frac{1}{\sqrt{R_{max}}} = 21.53659 + 0.019068a - 0.045552f - 5.00424 \times 10^{-4}n + 2.05619 \times 10^{-3}af - 1.14408 \times 10^{-3}a^2 + 3.0687 \times 10^{-9}n^2 \quad (12)$$

$$\frac{1}{\sqrt{R_t}} = 15.63583 + 0.01422a - 0.029091f - 3.6574 \times 10^{-4}n + 1.79178 \times 10^{-3}af - 9.46716 \times 10^{-4}a^2 + 2.24678 \times 10^{-9}n^2 \quad (13)$$

5.3 Analysis of variance

ANOVA of experimental data is always done to analyze statistically the relative significance of the models and its terms on the response. The parameters in the ANOVA are calculated as thus: sum of squares divided by degree of freedom (*df*) gives the mean square; "*F* values" which are tests of comparing models and their terms with a residual variance are calculated for a model and its terms by dividing respective mean square of the model and its terms with a residual mean square. If the variances are close to the same, the ratio will be close to 1 and it is less likely that any of the factors have significant effect on the response. Consequently, if a "*p* value" of any model and its terms is less than or equal to 0.05, the terms in the model have significant effect on the response.

Tables 4, 5, and 6 show the ANOVA studies for R_a, R_{max}, and R_t models in this research. For this work, Design Expert software has been used to generate the ANOVA results for the developed models. As shown in these tables, the models and their terms are significant at 95% confidence interval. The respective *p* values for the three models are less than 0.05 with the exception of depths of cut in R_{max} and R_t models as shown in Tables 5 and 6. Because there are strong interactions between depths of cut and feed rates in Tables 5 and 6, this justifies the inclusion of depth of cut in the developed models for the R_{max} in Eq. 12 and the R_t models in Eq. 13. Also, lack of fit tests for all the models in Tables 4, 5, 6 shows insignificance, indicating the response data fit the models well.

5.4 R_a model

Equation 11 is the second-order model that relates R_a with depth of cut, feed rate, and spindle speed at 95% confidence interval, while Table 4 shows the ANOVA study for the R_a model. As shown in Table 4, R_a model of "*F* value" of 72.66 indicates that the model is significant with less than 0.01% possibility of noise influence. By checking the *p* values and *F* values in Table 4, it is clearly seen that all the model terms are significant with spindle speed having the highest degree of significance followed by the feed rate and the interaction between depth of cut and feed rate. However, depth of cut has the lowest degree of significance

Table 4 ANOVA result for surface roughness (R_a) based on Box–Behnken method

Source	Sum of square	*df*	Mean square	*F* value	*p* value (*Prob*> *F*)	
Model	0.012000	5	0.00234900	72.66	<0.0001	Significant
a	0.0005915	1	0.00059510	18.41	0.0020	Significant
f	0.0012000	1	0.00120000	37.13	0.0002	Significant
n	0.0009461	1	0.00094610	29.26	0.0004	Significant
af	0.0006760	1	0.00067600	20.91	0.0013	Significant
n^2	0.0083290	1	0.00832900	257.60	<0.0001	Significant
Residual	0.0002910	9	0.00003233	–	–	–
Lack of fit	0.0002730	7	0.00003900	4.33	0.2003	Not significant
Pure error	0.0000180	2	0.00000900	–	–	–
Cor total	0.0120000	14	–	–	–	–

Prob Probability, *Cor total* Corrected total

Corrected total=Total Sum of squares (SS) for the model terms+residual SS and Corrected total=Sum of degrees of freedom (*df*) of all the model terms+residual *df*

Table 5 ANOVA result for surface roughness (R_{max}) based on Box–Behnken method

Source	Sum of square	*df*	Mean square	*F* value	*p* value *(Prob> F)*	
Model	0.5100000	6	0.08500000	84.53	<0.0001	Significant
a	0.0049510	1	0.00495100	4.91	0.0575	Significant
f	0.0440000	1	0.04400000	43.97	0.0002	Significant
n	0.0710000	1	0.07100000	70.50	<0.0001	Significant
af	0.0130000	1	0.01300000	13.27	0.0066	Significant
a^2	0.0150000	1	0.01500000	15.26	0.0045	Significant
n^2	0.3500000	1	0.35000000	346.95	<0.0001	Significant
Residual	0.0080650	8	0.00100800	–	–	–
Lack of fit	0.0079230	6	0.00132000	18.52	0.0521	Not significant
Pure error	0.0001400	2	0.00007131	–	–	–
Cor total	0.5200000	14	–	–	–	

Prob Probability, *Cor total* Corrected total

Corrected total=Total Sum of squares (SS) for the model terms+residual SS and Corrected total=Sum of degrees of freedom (*df*) of all the model terms+residual *df*

on the R_a. The lack of fit test of *F* value of 4.33 is not significant, indicating that all the data fit the model adequately in this study.

The influence of spindle speed is illustrated in Fig. 10. It can be clearly seen that R_a increases quadratically with an increase in spindle speed until 80,000 rpm. Further increase in spindle speed leads to a decrease in R_a in a quadratic fashion. This shows that lower spindle speed improves R_a. The effect of feed rate on R_a is dependent on the levels of depth of cut since there is a strong interaction between them. Montgomery et al. [26] have explained that whenever a strong interaction exists between two factors, the corresponding effects of the main factors have little or no practical significance. The interaction effect between feed rate and depth of cut on R_a is shown in Fig. 11. From Fig. 11a which depicts this interaction in 2D, it can be observed that R_a changes dramatically at different rates as the depth of cut increases from 5 to 20 μm for different levels of feed rate. This authenticates that a strong interaction exists between depth of cut and feed rate in this study. The combined effect of depth of cut and feed rate can be more visualized in Fig. 11b where it is shown in 3D form.

Equation 11 shows mathematically that R_a will increase when depth of cut, feed rate, and spindle are increased, but

Table 6 ANOVA result for surface roughness (R_t) based on Box–Behnken method

Source	Sum of square	*df*	Mean square	*F* value	*p* value *(Prob> F)*	
Model	0.2500000	6	0.04200000	78.38	<0.0001	Significant
a	0.0013800	1	0.00138000	2.56	0.1482	Significant
f	0.0050410	1	0.00504100	9.36	0.0156	Significant
n	0.0310000	1	0.03100000	58.15	<0.0001	Significant
af	0.0100000	1	0.01000000	18.86	0.0025	Significant
a^2	0.0110000	1	0.01100000	19.55	0.0022	Significant
n^2	0.1900000	1	0.19000000	348.09	<0.0001	Significant
Residual	0.0043090	8	0.00053870	–	–	–
Lack of fit	0.0042060	6	0.00070110	13.65	0.0698	Not significant
Pure error	0.0001027	2	0.00005136	–	–	–
Cor total	0.2600000	14	–	–	–	

Prob Probability, *Cor total* Corrected total

Corrected total=Total Sum of squares (SS) for the model terms+residual SS and Corrected total=Sum of degrees of freedom (*df*) of all the model terms+residual *df*

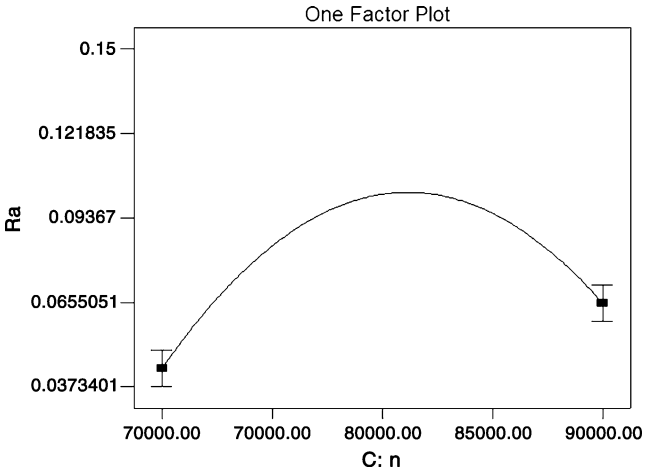

Fig. 10 Variation of R_a with spindle speed

it is improved with decrease in the square of spindle speed and the interaction of depth of cut and feed rate. Since from Fig. 10 it has been established that lowest spindle speed improves R_a, and the interaction between depth of cut and feed rate has been confirmed in Fig. 11a, then the combined effect of depth of cut and feed rate is shown in Fig. 12. Figure 12 shows the contour plot of the combined effect of depth of cut and feed rate on R_a at 70,000 rpm. From this figure, it can be seen that high depth of cut and moderate level of feed rate favor low R_a at 70,000 rpm. It follows therefore that R_a is improved with increase in depth of cut, medium feed rate, and decrease in spindle speed. This is in line with our conclusion in Section 5.1. Therefore, high depth of cut, moderate feed rate, and low spindle speed improve R_a in this work. R^2_{adj} for R_a model has been calculated as 96.3%. Specifically, 96.3% of the observed variability in the reduction R_t model can be explained by the model terms in Table 4.

5.5 R_{max} model

Equation 12 represents the R_{max} model. The R_{max} responses require inverse square root power transformation. This transformation is carried out using Box–Cox plotting technique available in Design Expert software. The

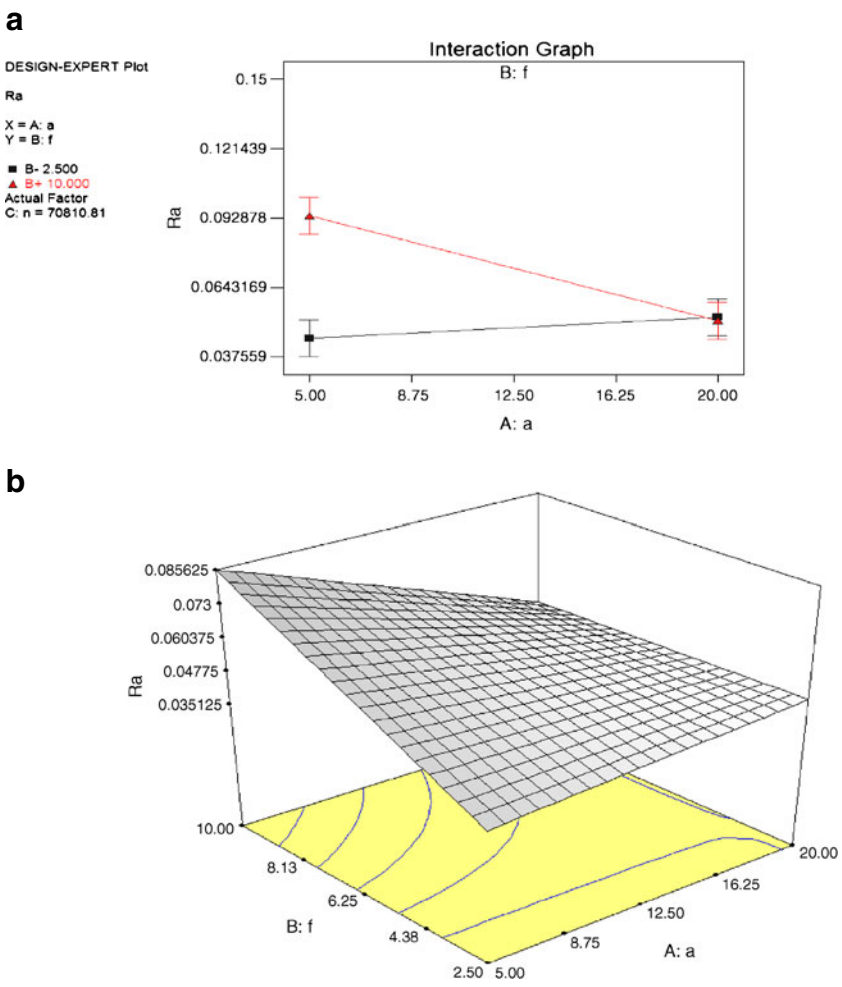

Fig. 11 The interaction between depth of cut and feed rate in R_a model at spindle speed of 70,000 rpm (**a**), 2D plot (**b**), and 3D response surface plot

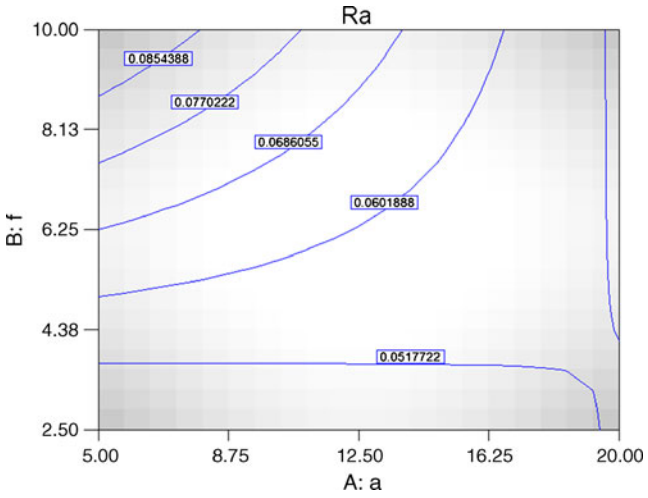

Fig. 12 Contour plot showing the combined effect of depth of cut and feed rate on R_a at spindle speed of 70,000 rpm

ANOVA study for this model is shown in Table 5. From Table 5, it is shown that R_{max} model of "F value" equal to 84.53 indicates that the model is significant with negligible noise. The p values of all the model terms are less than 0.05 except depth of cut. This shows that the terms are statistically significant. Since the p values for the square of depth of cut and the interaction of depth of cut and feed rate are less than 0.05, this makes the inclusion of depth of cut in R_{max} model in Eq. 12 inevitable. From Table 5, spindle speed, feed rate, depth of cut, and the interaction between depth of cut and feed rate affect R_{max} model in a decreasing degree of significance. The lack of fit test of F value of 18.52 is not significant, indicating that all the data fit the model adequately in this study.

The effect of spindle speed on the transformed scale of R_{max} is depicted in Fig. 13. It can be observed that the transformed scale of R_{max} decreases quadratically with an

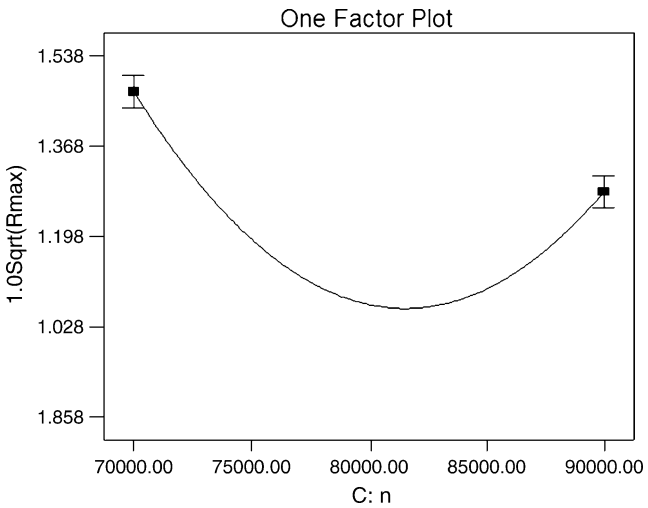

Fig. 13 Variation of R_{max} with spindle speed

increase in spindle speed up to 80,000 rpm and then increases quadratically as spindle speed changes from 80,000 to 90,000 rpm. This implies that moderate spindle speed improves the R_{max} better. In Eq. 12, there is a strong interaction between the depth of cut and feed rate which renders their respective main effects on R_{max} negligible. The interaction is shown in Fig. 14. From this figure, it can be seen that as the depth of cut increases from 5 to 20 μm, the transformed R_{max} decreases at 2.5 mm/min feed rate but increases at 10 mm/min feed rate indicating an existence of interaction between the depth of cut and feed rate (Fig. 14a). Figure 14b shows the 3D plot of this interaction. Figure 15 shows the contour plot for the combined influence of depth of cut and feed rate at 80,000 rpm on R_{max}. From this contour plot, it is observed that high depth of cut and moderate feed rate lead to low R_{max} (better surface roughness). Unlike R_a model, high depth of cut, moderate feed rate, and moderate spindle speed improve R_{max} in this work. R^2_{adj} for R_{max} model is 97.28%. This indicates that the model terms in Table 5 contribute about 97.28% in the observed variability in the reduction of R_{max} model.

5.6 R_t model

R_t model is shown in Eq. 13. The required transformation for the R_t is also the inverse square root, and Table 6 shows the ANOVA for this work. From this table, it can be observed that the p values for the feed rate, spindle speed, the interaction between depth of cut and feed rate, depth of cut and spindle speed are less than 0.05, indicating that these model terms are significant with spindle speed having the highest degree of significance. However, the p value for the depth of cut is greater than 0.05 indicating its non-significance in the R_t developed model. Nevertheless, since the p values of the interaction between depth of cut and feed rate and the square of depth of cut are less than 0.05, this has enabled the inclusion of the depth of cut in the R_t model. Invariably, all the model terms are significant factors indicating that the R_t model is adequate. The lack of fit test of F value of 13.6 is not significant, indicating that all the data fit the model adequately in this study

Figure 16 shows the variation of the transformed scale R_t with respect to spindle speed. From this figure, it can be observed that the transformed scale of R_t decreases quadratically with an increase in spindle speed up to 80,000 rpm and then increases quadratically as spindle speed changes from 80,000 to 90,000 rpm. This shows that the moderate level of spindle speed favors low transformed scale R_t. There exists an interactive effect between depth of cut and feed rate in Eq. 13. The authentication of this interaction is shown in Fig. 17. As can be seen in Fig. 17a, there is a strong interaction between the depth of cut and

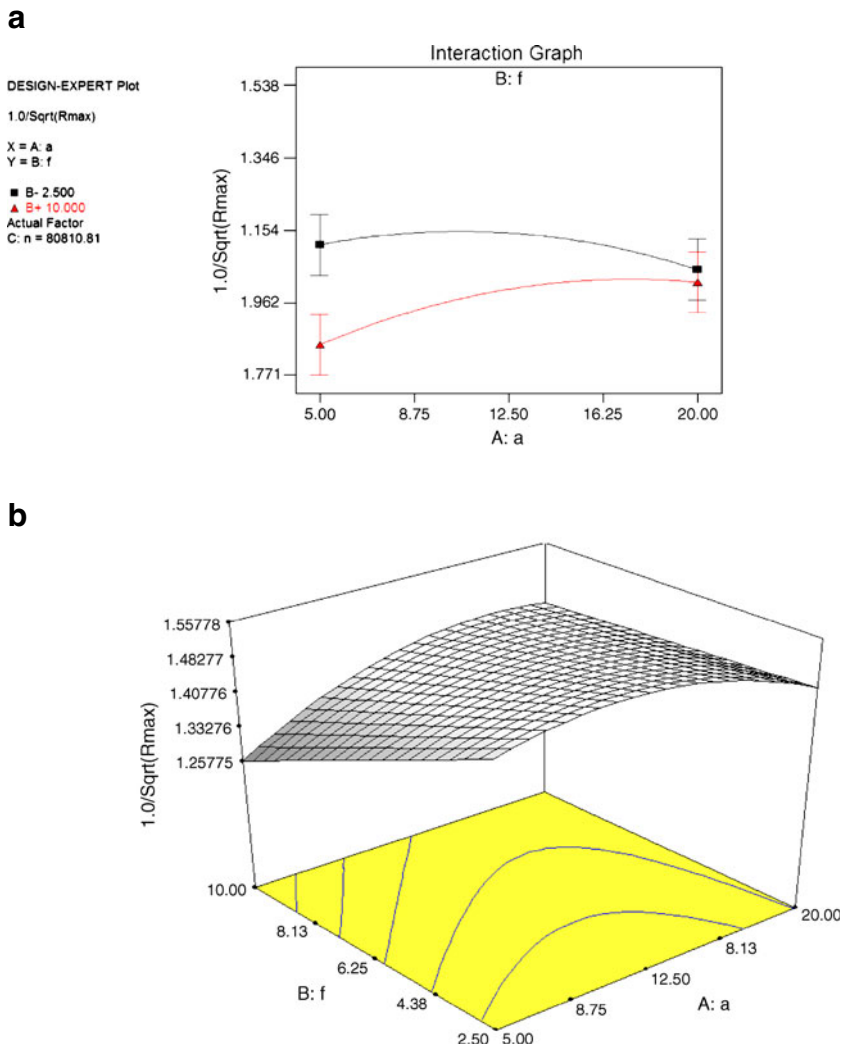

Fig. 14 The interaction between depth of cut and feed rate in R_{max} model at spindle speed of 80,000 rpm (**a**), 2D plot (**b**), 3D response surface plot

feed rate and these two parameters combine together to influence R_t. Figure 17b shows the 3D view of the interaction between depth of cut and feed rate. Figure 18 shows the contour plot for the combined influence of depth of cut and feed rate at 80,000 rpm on R_t. From this figure, it

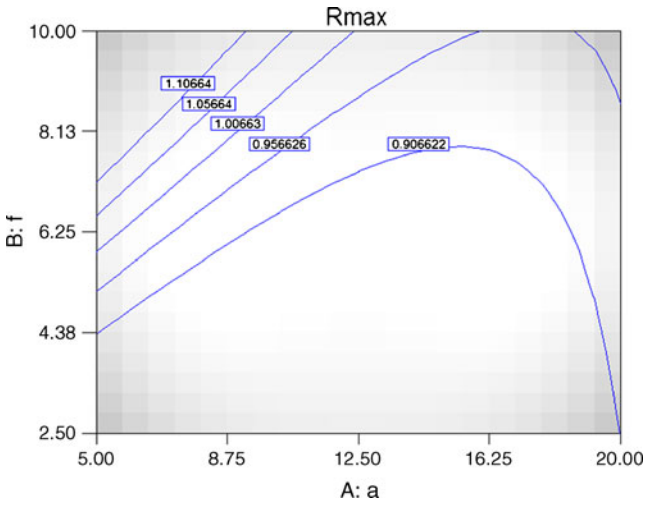

Fig. 15 Contour plot showing the combined effect of depth of cut and feed rate on R_{max} at spindle speed of 80,000 rpm

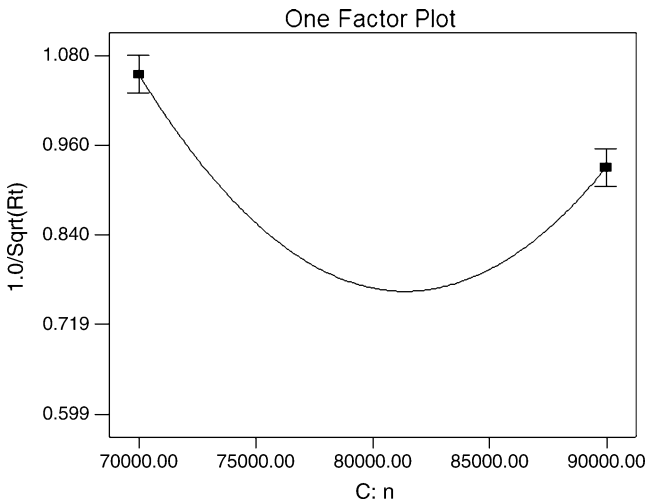

Fig. 16 Variation of R_t with spindle speed

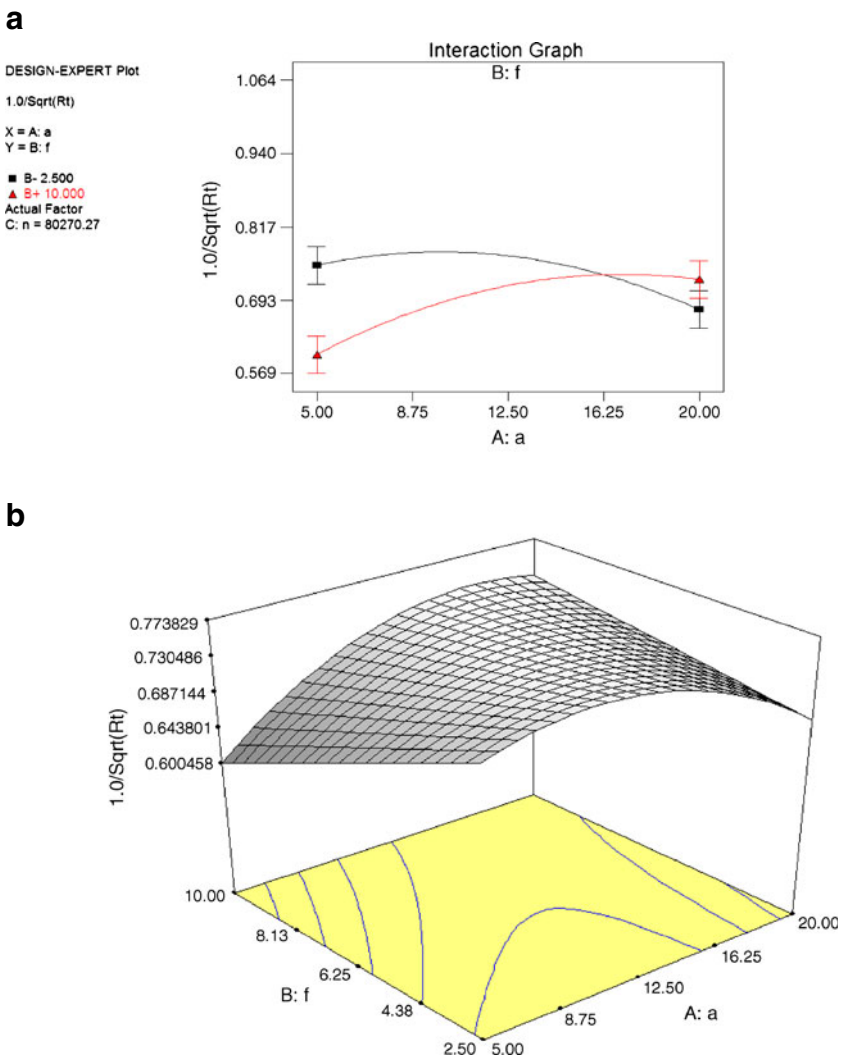

Fig. 17 The interaction between depth of cut and feed rate in R_t model at spindle speed of 80,000 rpm (**a**), 2D plot (**b**), 3D response surface plot

can be observed that high depth of cut improves the surface roughness R_t while feed rate has little or no influence on the

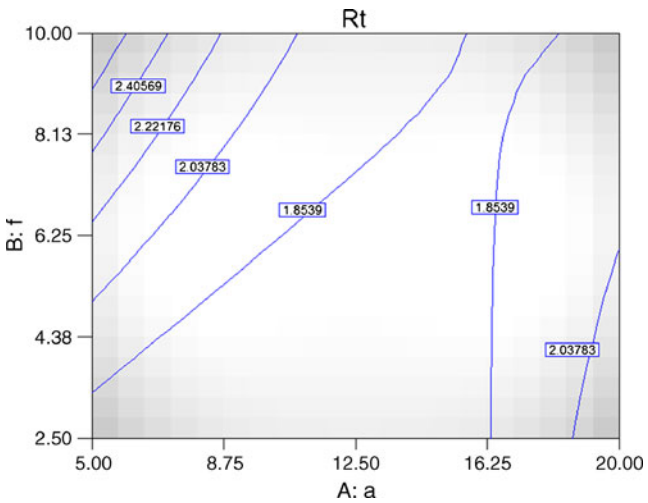

Fig. 18 Contour plot showing the combined effect of depth of cut and feed rate on R_t at spindle speed of 80,000 rpm

transformed scale of R_t. R^2_{adj} for R_t model is 97.03%, indicating the model terms in Table 6 can contribute about 97.03% in the variability observed in the reduction of R_t model.

5.7 Optimization experiments

The developed surface finish models are used for multiple response optimizations by desirability function to obtain

Table 7 Set criteria for optimization experiments used in this study

Grinding parameter	Goal	Lower limit	Upper limit
Depth of cut (μm)	Is in range	5.0	20
Feed rate (mm/min)	Is in range	2.5	10
Spindle speed (rpm)	Is in range	70,000	90,000
R_a (μm)	Minimize	0.043	0.150
R_{max} (μm)	Minimize	0.423	1.358
R_t (μm)	Minimize	0.883	2.790

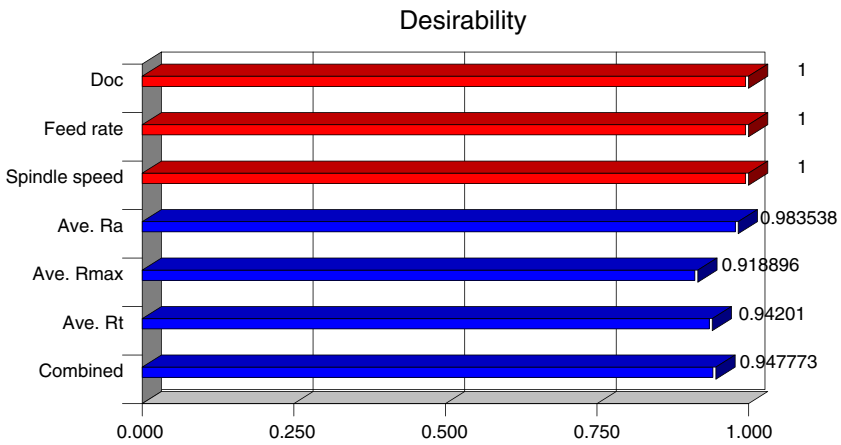

Fig. 19 Histogram showing the maximum desirability of 0.95 for the combined objective

minimum surface roughness for R_a, R_{max}, and R_t using the set criteria in Table 7 and the desirability function in Eq. 6. After using Design Expert software, the maximum desirability is found to be 95% (Fig. 19). This corresponds to the optimum condition of depth of cut, 17.5 μm; feed rate, 5 mm/min and spindle speed, 70,000 rpm as detailed by Alao [35]. This was predicted to lead to the generation of ground surfaces with 40-nm R_a, 420-nm R_{max}, and 882-nm R_t expected on precision ground silicon surfaces. Experiments conducted to confirm this prediction generated 37-nm R_a, 400-nm R_{max}, and 880-nm R_t on silicon ground surfaces. Figure 20 shows the optical and SEM images of silicon surface observed after performing optimization experiments. Figure 20 illustrates the largest ductile surfaces possible observed in this study after performing optimization tests based on desirability function in Eq. 6 and the set criteria for optimization experiments in (Table 7). In this study, Fig. 20 are obtained under the optimized condition of depth of cut of 17.5 μm, feed rate of 5 mm/min, and spindle speed of 70,000 rpm, and these conditions generated massive ductile-streaked surfaces with a surface finish of 37-nm R_a, 400-nm R_{max}, and 880-nm R_t. This clearly shows some improvements in surface finishes and larger amounts of ductile streaks on precision ground surfaces of silicon in comparison to Fig. 8a. Consequently, faster polishing action can be achieved on this ground surfaces than in Fig. 8a. Also, surface finish of 37-nm R_a meets the ophthalmic conditions where the tolerance of the profile is not stringent, but the surface finish has to be on the order of a nanometer for cosmetic purposes [3, 10].

6 Conclusions

Box–Behnken design has been used for precision grinding of silicon in this investigation. Using grinding process parameters depths of cut, feed rates, and spindle speeds, prediction models have been developed for surface roughness parameters R_a, R_{max}, and R_t in precision grinding process with resin-bonded grinding pins. Optimization by desirability function has been performed to obtain the

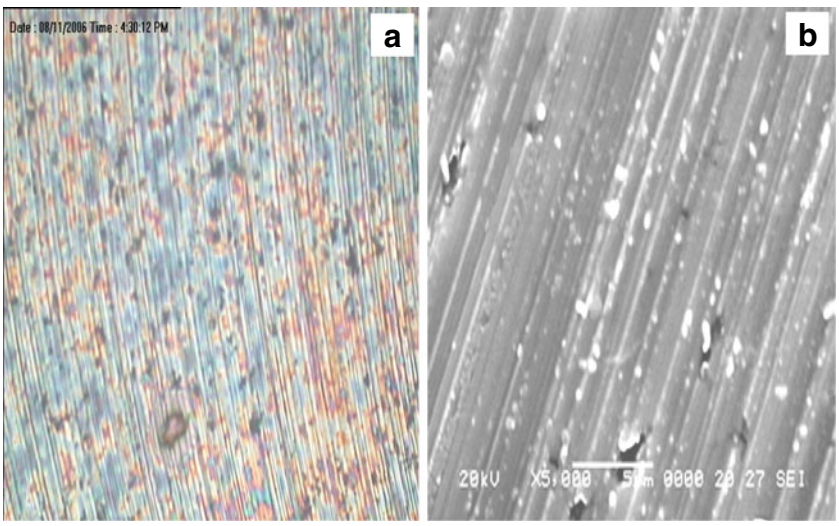

Fig. 20 Images of silicon surfaces after performing optimization experiments with optimum conditions of depth of cut of 17.5 μm, feed rate of 5 mm/min, and spindle speed of 70,000 rpm: **a** optical micrograph, **b** SEM

optimum precision grinding conditions. In the light of our analysis, the following conclusions can be drawn.

1. Massive ductile surface has been generated on ground silicon material at depth of cut of 20 μm, feed rate of 6.25 mm/min, and spindle speed of 70,000 rpm with a 43-nm R_a. This indicates that larger amounts of ductile streaks can be achieved by properly selecting the precision grinding conditions.
2. Second-order models have been developed for surface parameters R_a, R_{max}, and R_t for precision grinding of silicon within the experimental region depth of cut (5–20 μm), feed rate (2.5–10 mm/min), and spindle speed (70,000–90,000 rpm). These models are capable of navigating the design space.
3. In this work, R^2_{adj} are 96.3%, 97.28%, and 97.03% for R_a, R_{max}, and R_t models, respectively. It is clearly seen that the roughness data measured from the experiments are sufficient to build other prediction models.
4. The optimization experiments based on desirability function predict a ground surface with 40-nm R_a, 420-nm R_{max}, and 882-nm R_t, and the confirmation experiments show 37-nm R_a, 400-nm R_{max}, and 880-nm R_t indicating an improvement in the surface roughness of 7.5%, 4.8%, and 0.23% in R_a, R_{max}, and R_t, respectively. Therefore, Box–Behnken design is a useful tool for modeling and prediction of precision grinding processes.
5. SEM surface of precision ground surface at the confirmation experiment reveals larger amounts of ductile streaks in comparison to Fig. 8a, thereby reducing the polishing time and meeting the ophthalmic conditions where the tolerance is not stringent, but the surface finish has to be on the order of a nanometer for cosmetic purposes [3,10].
6. We have also been able to demonstrate in this study that by proper selection of precision grinding conditions, massive ductile streaks with a roughness as low as 37-nm R_a can be achieved on a general purpose NC milling without the need for a purposely built surface grinder.

References

1. Fang FZ, Venkatesh VC (1998) Diamond cutting of silicon with nanometric finish. CIRP Ann 47(1):45–49
2. Shibata T, Fujii S, Makino E, Ideda M (1996) Ductile-regime turning mechanism of single-crystal silicon. Prec Eng 18:129–137
3. Venkatesh VC, Fang F, Chee WK (1997) On mirror surfaces with and without polishing. CIRP Ann 46(1):505–508
4. Komanduri R, Lucca DA, Tani Y (1997) Technological advances in fine abrasive processes. CIRP Ann 46(2):545–596
5. Rahman M, Senthil AK, Lim HS, Fatima K (2003) Nano finish grinding of brittle materials using electrolytic in-process dressing (ELID) technique. Sadhana 28(5):957–974
6. Zhang B, Yang F, Wang J, Zhu Z, Monahan R (2000) Stock removal rate and workpiece strength in multi-pass grinding of ceramics. J Mater Process Technol 104:178–184
7. Blackley WS, Scattergood RO (1991) Ductile-regime machining model for diamond turning of brittle materials. Prec Eng 13 (2):95–102
8. König W, Sinhoff V (1992) Ductile grinding of ultra-precise aspherical optical lenses. SPIE, Lens and Optical Systems Design 1780:778–788
9. Zhong ZW (2003) Ductile or partial ductile mode machining of brittle materials. Int J Adv Manuf Technol 21:579–585
10. Ong NS, Venkatesh VC (1998) Semi-ductile grinding and polishing of Pyrex glass. J Mater Process Technol 83:261–266
11. Venkatesh VC, Izman S, Sharif S, Mon TT, Konneh M (2003) Ductile streaks in precision grinding of hard and brittle materials. Sadhana 28(5):915–924
12. Venkatesh VC, Izman S (2007) Development of a novel binderless diamond grinding wheel for machining IC chips for failure analysis. J Mater Process Technol 185:31–37
13. Izman S, Venkatesh VC (2007) Gelling of chips during vertical surface diamond grinding of BK7 glass. J Mater Process Technol 185:178–183
14. Venkatesh VC, Izman S, Vichare PS, Mon TT, Murugan S (2005) The novel bondless wheel, spherical glass chips and a new method of aspheric generation. J Mater Process Technol 167:184–190
15. Liu JH, Pei ZJ, Graham RF (2007) ELID grinding of silicon wafers: a literature review. Int J Mach Tool Manuf 47:529–536
16. Thomas TR (1999) Rough surface. Imperial College Press, London
17. Inasaki I (1987) Grinding of hard and brittle materials. CIRP Ann 36(2):463–471
18. Bridgman PW (1953) Effects of very high-pressure on glass. J Appl Physics 24:405–413
19. Komanduri R, Chandrasekaran N, Raff LM (2001) Molecular dynamics simulation of nanometric cutting of silicon. Philos Mag 81(12):1989–2019
20. Fang FZ, Zhang GX (2003) An experimental study of edge radius effect on cutting single crystal silicon. Int J Adv Manuf Technol 22:703–707
21. Shaw MC (1995) Precision finishing. Ann CIRP 44(1):343–348
22. Liu K, Li X, Liang SY, Liu XD (2004) Nanometer scale ductile mode cutting of soda-lime glass. Trans NAMRI/SME 32:39–45
23. Liu K, Li X, Liang XY, Liu XD (2005) Nanometer-scale, ductile-mode cutting of soda-lime glass. J Manuf Process 7 (2):95–101
24. Miyashita M (1989) Brittle/ductile machining. Fifth international seminar on precision engineering, Monterey, CA, USA
25. Masuzawa T, Tönshoff HK (1977) Three-dimensional micro-machining by machine tools. CIRP Ann 46:621–628
26. Montgomery DC, Runger GC, Hubele NF (1998) Engineering statistics. Wiley, New York
27. Krajnik P, Kopac J, Sluga A (2005) Design of grinding factors based on response surface methodology. J Mater Process Technol 162–163(SPEC ISS):629–636
28. Alao A-R, Konneh M (2009) A response surface methodology based approach to machining processes: modelling and quality of the models. Int J Exp Des Process Optim 1(2/3):240–261
29. Derringer G, Suich R (1980) Simultaneous optimization of several response variables. J Qual Technol 12(4):214–219

30. Stephenson DA, Agapiou JS (1997) Metal cutting theory and practice. Marcel Dekker, New York
31. Rusnaldy, Ko TJ, Kim HS (2008) An experimental study on microcutting of silicon using a micromilling machine. Int J Adv Manuf Technol 39:85–91
32. Matsuo T, Touge M, Yamada H (1997) High-precision surface grinding of ceramics with superfine grain diamond cup wheel. CIRP Ann 46(1):249–252
33. Routara BC, Bandyopadhyay A, Sahoo P (2009) Roughness modeling and optimization in CNC end milling using response surface method: effect of workpiece material variation. Int J Adv Manuf Technol 40:1166–1180
34. Fang N (2005) Tool-chip friction in machining with a large negative rake angle tool. Wear 258:25–29
35. Alao AR (2007) Precision micro-scaled partial ductile mode machining of silicon. Dissertation, International Islamic University Malaysia